Origin and fate of sulfide liquids in hotspot volcanism (La Réunion): Pb isotope constraints from residual Fe–Cu oxides

Ivan Vlastélic, Abdelmouhcine Gannoun, Andréa Di Muro, Lucia Gurioli, Patrick Bachèlery, Jean-Marc Hénot

Origin and fate of sulfide liquids in hotspot volcanism (La Réunion): Pb isotope constraints from residual Fe–Cu oxides

I. Vlastélic [a,*], A. Gannoun [a], A. Di Muro [b], L. Gurioli [a], P. Bachèlery [a], J.M. Henot [a]

[a] *Laboratoire Magmas et Volcans, CNRS UMR 6524, Université Blaise Pascal, Clermont-Ferrand, France*
[b] *Observatoire Volcanologique du Piton de la Fournaise, Institut de Physique du Globe, Sorbonne Paris-Cité, CNRS UMR 7154, Université Paris Diderot, Paris, France*

Immiscible sulfide liquids in basaltic magmas play an important role in trace metal transport and the sulfur budget of volcanic eruptions. However, sulfides are transient phases, whose origin and fate are poorly constrained. We address these issues by analyzing sulfide destabilization products preserved in lavas from La Réunion Island. Iron oxide globules and coatings, typically 20–80 μm in size, were found to occur in vesicles of differentiated lavas from Piton des Neiges, and recent pumice samples from Piton de la Fournaise. Field and mineralogical evidence indicates that the iron oxides are syn-eruptive phases not resulting from hydrothermal processes. Samples were first studied by Scanning Electron Microscopy. The globules were separated, whereas the smaller spherules and coatings were concentrated by magnetic sorting and acid leaching, and samples were processed through wet chemistry. The Fe oxide phases comprise 49–74 wt.% Fe, 26–40 wt.% O, and up to 6 wt.% Cu, 811 ppm Ni, 140 ppm Bi, and 8.5 ppm Pb. Compared to the host lava, Cu, Ni, and Bi are enriched by a factor of 10^1–10^3. Systematic Pb isotope disequilibrium (between 500 ppm and 2.9% for $^{206}Pb/^{204}Pb$) exists between Fe oxides and host rocks, with Fe oxides generally displaying less radiogenic ratios. Unradiogenic Pb is a typical signature of sulfide, which tends to concentrate Pb, but not its parent elements U and Th. Thus, both the chemical and isotopic compositions of the vesicle-hosted Fe oxides suggest that they are more or less direct products of the destabilization of immiscible sulfide liquids. Although Pb dominantly partitions into the gas phase during sulfide breakdown, the original Pb isotope signature of sulfide is preserved in the residual oxide. The composition estimated for the parent sulfides ($^{206}Pb/^{204}Pb = 18.20$–$18.77$, $^{207}Pb/^{204}Pb = 15.575$, and $^{208}Pb/^{204}Pb = 38.2$–38.8) precludes a genetic link with the La Réunion plume, and suggests a lithospheric or crustal origin.

It is estimated that magma ascent velocities at Piton de la Fournaise are high enough to counterbalance the settling velocities of millimeter-size sulfides. Despite their high density, sulfide liquids are thus transferred upward during eruptions and their destabilization contributes to SO_2 emanations. Assimilation of foreign sulfides from the lithosphere can explain why SO_2 emissions sometimes (e.g., during the April 2007 eruption) exceed those predicted from the S content of melt inclusions.

Keywords: Sulfide; Magma degassing; Pb isotopes; Piton de la Fournaise

1. INTRODUCTION

There is natural and experimental evidence that many pre-eruptive basaltic magmas are sulfide saturated (Métrich and Clochiatti, 1996; Jugo et al., 2005). Sulfide exsolution plays an important role in maintaining low

* Corresponding author.
E-mail address: i.vlastelic@opgc.univ-bpclermont.fr (I. Vlastélic).

concentrations of dissolved sulfur (ca. 1400 ppm at Fayalite-Magnetite-Quartz (FMQ) redox buffer, Jugo et al., 2005) and preventing SO_2 accumulation (Wallace and Edmonds, 2011). However, sulfide saturation makes the sulfur budget of pre-eruptive magmas difficult to estimate because both the amount of exsolved sulfide and the fate of sulfides are poorly constrained. Sulfide liquids are generally scarce in sub-aerial lavas, and mostly occur as heterogeneous secondary Fe–Cu–Ni sulfide globules in olivine melt inclusions (Clocchiatti et al., 1979; Di Muro et al., 2014) and in quenched lava samples (Moore and Calk, 1971; Stone and Fleet, 1991). It thus remains unclear whether sulfide saturation is a secondary process, or if it is an active process in high temperature melts producing early S depletion in the plumbing system (Mavrogenes and O'Neill, 1999; Collins et al., 2012). The fate of immiscible sulfides during magma ascent, eruption and degassing is at the heart of this issue: because sulfide liquids are denser than silicate melt, they are expected to settle gravitationally and accumulate in the fractionated solid phase, thus escaping the degassing process. For instance, it is estimated that settling sulfide liquids represent 20–90% and 50% of the sulfur budget at Piton de la Fournaise (La Réunion) and Grimsvötn (Iceland) volcanoes, respectively (Collins et al., 2012; Sigmarsson et al., 2013). Alternatively, sulfides may ascend, possibly attached to gas bubbles (Mungall et al., 2015), and, following magma oxidation, dissolve into the silicate melt, or destabilize into Fe oxides and a fluid phase to which trace metals are transferred (Clarke, 1911; Larocque et al., 1998, 2000; Di Muro et al., 2008; Berlo et al., 2014). The importance of such processes in controlling chalcophile element transport and ore deposit formation in subduction zone settings is well established (Sun et al., 2015; Nadeau et al., 2010, 2013; Lee et al., 2012).

It is estimated that mantle sulfide remains a solidus phase until ca. 20% partial melting (Rehkämper et al., 1999), although this value depends on the sulfur content of the mantle, the oxidation state and the melt composition (O'Neill and Mavrogenes, 2002). It is likely that low degree melts produced in intraplate settings are initially in equilibrium with residual sulfide. However, because the solubility of sulfide in silicate melts increases with decreasing pressure, melts will evolve away from sulfide saturation during ascent (Mavrogenes and O'Neill, 1999; Hart and Gaetani, 2006). A major implication is that these sulfide undersaturated melts will tend to assimilate genetically unrelated sulfides as they rise through the lithosphere and crust (Di Muro et al., 2008; Hart and Gaetani, 2006). Sulfides trapped in abyssal peridotites display large Pb and Os isotopic variations (Harvey et al., 2006; Burton et al., 2012; Warren and Shirey, 2012; Blusztajn et al., 2013) that record a long history of storage and/or recycling. Assimilation of such sulfides by ascending plume melts is expected to strongly influence the S budget of primary magmas as well as their Pb and Os isotope signatures (Hart and Gaetani, 2006).

Réunion Island volcanism (Indian Ocean) samples a sulfide saturated magmatic reservoir (Métrich and Clochiatti, 1996; Upton et al., 2000), and, as elsewhere, sulfides are rarely transferred to and/or preserved in the erupted lavas. Common occurrences of sulfide globules have been reported in the interstitial glass of wherlitic and gabbroic cumulates entrained during a major explosive event of Piton de la Fournaise 4700 years ago, which produced the Bellecombe Ash deposit (Upton et al., 2000), raising the possibility that sulfides accumulate in the plutonic roots of the volcano (Collins et al., 2012). However, these globules are too Ni-rich to be in equilibrium with the evolved glasses, and contain less S (S $<$38 wt.%) than sulfides formed in melt inclusions by post entrapment processes (S $>$45 wt.%). Furthermore, Di Muro et al. (2014) noted that sulfur and chalcophile element co-variations in melt inclusions from the April 2007 eruption are consistent with melt degassing, without major contributions from sulfides. To decipher whether sulfides sink or contribute to SO_2 emanation, this study tracks sulfide fingerprints in erupted lavas, in particular in quenched samples where sulfide remnants are best preserved (Larocque et al., 2000). Our approach relies on Pb isotopes, which are expected to remain unfractionated during sulfide destabilization, although a large fraction of the lead present in sulfide is transferred to the fluid and gas phases (Berlo et al., 2014). The Pb isotopic composition of sulfide destabilization products might also provide information on the origin and history of the parent sulfides.

2. SAMPLES AND METHODS

A first sample (PDN17) was selected for this study based on the abundance of iron-rich globules in vesicles. This sample belongs to the 350–230 ka old differentiated series of Piton des Neiges, where extensive magnetite fractionation might have triggered massive sulfide exsolution (Collins et al., 2012). This is a plagioclase-phyric basalt with 4.0 wt.% MgO, 18.85 wt.% Al_2O_3 and 45.8 wt.% SiO_2 (Smietana, 2011). Loss on ignition (0.68) is within the range reported for fresh Réunion samples. Other samples are from the very recent (2010–2015) eruptions of Piton de la Fournaise. Their compositions are transitional between the tholeitic and alkali fields, as are most samples erupted since 0.5 Ma, and show little variability (MgO between 6.2 and 6.7 wt.%). This study focuses on air-quenched spatters; artificially quenched samples were not considered because they are potentially contaminated with the iron-made sampling tools. All samples were collected during eruptions, with the exception of samples 141118-x, which were collected five months after emplacement. All spatters have negative loss on ignition (from -0.9 to -0.3) indicating that samples are not oxidized. A subset of 2014 samples was studied for texture and crystal content (Gurioli et al., 2015). They include, in the order of decreasing density and crystal content, spiny scoria, fluidal scoria, low-density fluidal scoria and golden pumice. The low-density fluidal and golden textures reflect less degassed magmas that ascended and cooled rapidly.

Samples were surveyed by Scanning Electron Microscopy (SEM) operating in Backscattered Electron (BSE) and Secondary Electron (SE) imaging modes. Semi-quantitative compositions of iron-rich phases lying on vesicles walls were determined using Energy Dispersive

Spectrometry (EDS). Globules of sample PDN17 were taken off from vesicle walls with a micro-needle, rinsed with ultra-pure (UP) water. Between 0.032 and 0.035 mg (3–6 globules) were weighed with a Mettler microbalance and dissolved in a mixture of UP 16 M HNO_3 and 30 M HF for wet chemistry analysis. The HNO_3-HF mixture was used following preliminary tests showing that, unlike magmatic magnetite, iron oxide globules dissolved very slowly in HNO_3 or HCl. A disadvantage of this method is that HF also dissolved a small fraction of silicate attached to the globules (10–25%, see Section 3.2.1.). Most iron oxides hosted in vesicles of recent samples from Piton de la Fournaise were too small to be separated. They were concentrated by physical and chemical means: between 10 and 20 g of soft glassy material was gently crushed in an agate mortar to obtain a coarse powder. In a first approach, the glass chips hosting Fe oxides were picked manually with a magnet. This method was efficient for truly glassy samples (golden pumice) that do not contain post eruptive magnetite crystals. The isolated magnetic fractions (0.06–7.3 mg) were weighed and dissolved in 16 M HNO_3 – 30 M HF (0.2 ml of each), dried, and re-dissolved in 1 ml of 3 M UP HNO_3. In a second approach, the crushed samples (300 mg) were rinsed with water (5 min in an ultrasonic bath) and the Fe oxides were leached with 1.4 ml of 3 M UP HNO_3 for 10 min at room temperature in an ultrasonic bath. Uncrushed chips were also leached for comparison. A weighed aliquot (10%) of the sample solutions (globule separates, magnetic fractions, and acid leachates) was used to measure trace element concentrations via an Agilent 7500 Inductively Coupled Plasma Mass Spectrometer (ICP-MS). The remaining fraction was processed through Pb isotope chemistry, as well as a subset of the leaching residues.

The separation method used solutions with varying HBr concentration (0.2–0.03 M) in 0.5 M HNO_3 media to control Pb retention on anionic resin (AG1-X8; Vlastélic et al., 2013). This method has been improved in two ways. (1) Small volumes of concentrated HBr were distilled just prior to Pb separation using an Analab evapoclean device. (2) Instead of evaporating sample solutions between the first and second chemistry, 20 µl of freshly distilled 8.75 M HBr were added to the 1 ml Pb fraction eluted during the first chemistry in order to increase HBr concentration from 0.03 M to 0.2 M. These improvements decreased the total Pb blank from 6 to 7 pg at the beginning of this study to 1.7–3.0 pg ($n = 3$) and enabled the analysis of small amounts of Pb. Lead isotopic compositions were measured on a Neptune Plus multiple collector ICPMS (Laboratoire Magmas et Volcans) set up for high sensitivity on heavy masses (large interface pump, Jet sample cone and a X-skimmer cone). A 10^{12} Ω resistor was used to enhance the ^{204}Pb signal-to-noise ratio. The amount of lead separated from samples ranged from 74 pg to 114 ng. When 1 ng or more Pb was available, lead was diluted in UP 0.05 N HNO_3 and spiked with Tl NBS997 to obtain 1 ml solutions with compositions ranging from 5 ppb Pb – 1 ppb Tl (Pb/Tl = 5) to 1 ppb Pb – 0.5 ppb Tl (Pb/Tl = 2). The solutions were introduced through an Aridus II desolvating nebulizer system at a rate of 100 µl/min yielding a total Pb beam of 10 to 12.10^{-11} A for 5 ppb Pb solutions. Data were corrected for instrumental mass fractionation using Tl. Repeated analysis of the NBS981 standard every two samples yielded typical intra session reproducibility of 100, 120 and 140 ppm (2σ) for $^{206}Pb/^{204}Pb$, $^{207}Pb/^{204}Pb$ and $^{208}Pb/^{204}Pb$, respectively, comparable with the reproducibility obtained by lead triple spiking (Galer and Abouchami, 1998). The smallest samples (74–296 pg Pb) were dissolved in 0.3 ml of 0.05 M HNO_3 with a Pb/Tl ratio in the range of 0.5–1, and Pb isotopes were measured using a method consuming and measuring the entire sample solution. In this method, baseline and peak center measurements were performed on NBS981 just prior to and after sample measurement. Repeated analysis of NBS981 in the same conditions as the samples (300 pg in 0.3 ml) yielded a precision better than 200 ppm/amu. Lead compositions of samples with less than 300 pg Pb ($n = 3$) were corrected using a procedural blank, whose isotopic composition was measured regularly by leaving a beaker open in the clean room. The mean blank composition ($n = 4$) is $^{206}Pb/^{204}Pb = 18.347 \pm 0.202$, $^{207}Pb/^{204}Pb = 15.603 \pm 0.006$, and $^{208}Pb/^{204}Pb = 38.005 \pm 0.174$. Blank correction ranges from 2% to 6%. For each session, data were re-normalized to the NBS981 values of Todt et al. (1996) to be directly comparable with previously published data on lavas (Vlastélic et al., 2009).

3. RESULTS

Lead isotope compositions and Ni–Cu–Tl–Pb–Bi trace element data of the Fe oxides (globules, magnetic separates and leachates) are reported in Table 1. SEM data, including BSE and SE images and EDS compositions, the complete trace element data set, and whole rock reference compositions are reported as Supplementary material (Tables A, B and C, respectively).

3.1. Scanning Electron Microscopy

Spherules 50–100 µm in size are common in the vesicles of the differentiated sample (PDN17) from Piton des Neiges. Spherule surfaces show well-developed crystal faces, and some of the largest species show spiky outgrowths. Some globules have a spongy texture. Polished sections show a core composed essentially of iron oxide with 65–74% Fe, and an outer shell with 49–54% Fe, 30–34% O, 9–11% Mg and 3–5% Cu (Fig. 1a and Supplementary Table A). Titanium (1–3%) at the globule-silicate boundary probably originates from the host basalt. In recent glassy samples, iron oxides generally occur as thin coatings (<1 µm) on vesicle walls. In sample 141118-6, iron oxides cluster in small (20–30 µm) pre-existing cavities (Fig. 1b). *In-situ* semi-quantitative analysis of Fe-oxides by EDS yields 50–65 wt.% Fe, 27–40 wt.% O and 0–6 wt.% Cu after correction for the background silicate signal (Supplementary Table A). These compositions compare well with those of the Fe–Cu oxide globules of sample PDN17. Sulfur was not detected in any samples. Inspection of the magnetic separates reveals that they are made of glassy fragments enriched in Fe oxides. A few larger

Table 1
Selected trace element data and Pb isotopic compositions of vesicle-hosted Fe oxides.

	Sample name	Eruption date	Sample type		Ni	Cu	Tl	Pb	Bi	$^{206}Pb/^{204}Pb$	$^{207}Pb/^{204}Pb$	$^{208}Pb/^{204}Pb$	ng Pb[1]	Blank correction[2]
					ppm	ppm	ppm	ppm	ppm	(±2σ)[2]	(±2σ)[2]	(±2σ)[2]		(%)
Separated globules	PDN17	350–230 ka BP	Differentiated lava	Batch A	364	12922	0.04	2.93	36	18.372 (0.027)	15.596 (0.025)	38.411 (0.061)	0.094	6.4
				Batch B	421	11575	0.04	8.46	140	18.378 (0.026)	15.590 (0.021)	38.403 (0.052)	0.296	2.0
Magnetic fractions	140624-3	Jun-14	Small glassy scoria		249	541	0.08	2.00	0.068	18.8868	15.5862	38.9617	5.99	
	140624-13a	Jun-14	Fluidal scoria		70	125	0.04	1.91	0.074	18.8986	15.5945	38.9942	14.0	
	141118-5-d	Jun-14	Spiny scoria		58	118	0.04	1.69	0.030	18.9004	15.5964	38.9987	3.34	
	141118-5-l	Jun-14	Low density fluidal scoria		68	111	0.03	1.56	0.051	18.8988	15.5953	38.9963	6.63	
	141118-3	Jun-14	Golden pumice		154	394	0.04	1.95	0.090	18.8852	15.5953	38.9774	1.37	
	150212-13	Feb-15	Golden pumice		113	295	0.38	2.01	0.057	18.8938	15.5884	38.9691	0.85	
	1012-136	Dec-10	Light lapillis		811	2175	–	1.23	0.154	19.454 (0.042)	15.655 (0.026)	39.021 (0.070)	0.074	4.1
	Sample name	Eruption date	Sample type		$EF^{(3)}_{(Ni)}$	$EF_{(Cu)}$	$EF_{(Tl)}$	$EF_{(Pb)}$	$EF_{(Bi)}$	$^{206}Pb/^{204}Pb$	$^{207}Pb/^{204}Pb$	$^{208}Pb/^{204}Pb$	ng Pb[1]	Blank correction[2]
										(±2σ)[2]	(±2σ)[2]	(±2σ)[2]		(%)
Acid leachates	1001-053	Jan-10	Glassy pumice	Uncrushed chip	0.75	3.21	1.71	2.23	18.4	18.9016	15.5951	38.9928	6.6	
				Crushed chip a	0.73	1.90	1.42	1.52	8.74	18.8819	15.5859	38.9477	10	
				” b	0.72	1.79	1.24	1.43	7.34	18.8859	15.5947	38.9727	12	
				” c	0.69	1.43	1.02	1.28	6.03	18.8972	15.5946	38.9872	22	
				” d	0.72	1.50	1.03	1.37	6.76	18.8977	15.5924	38.9804	18	
	140624-3	Jun-14	Small glassy scoria	Crushed chip a	0.56	1.12	3.36	0.94	1.62	18.8927	15.5916	38.9784	67	
				” b	0.51	1.20	4.59	0.95	2.02	18.8925	15.5988	38.9946	58	
				” c	0.54	2.23	12.9	1.20	4.56	18.8660	15.5972	38.9579	18	
				” d	0.47	1.92	11.8	1.17	5.54	18.8718	15.5927	38.9553	24	
				” e	0.67	1.00	2.69	0.91	1.24	18.8921	15.6009	39.0000	114	
				” f	0.90	1.43	5.15	0.99	2.07	18.8751	15.6009	38.9770	56	
				” g	0.51	1.89	12.8	1.16	5.09	18.8789	15.5971	38.9751	15	
				Uncrushed chip a	0.38	4.26	546	1.52	10.1	18.9013	15.5965	38.9991	6.0	
				” b	0.48	2.78	88.0	1.31	9.83	18.9019	15.5963	39.0025	9.5	
				” c	0.45	3.78	67.5	1.71	15.6	18.8982	15.5939	38.9904	5.4	
				” d	0.45	3.95	123	2.73	28.7	18.9004	15.5967	39.0016	6.4	
	141118-6	Jun-14	Glassy pumice	Uncrushed chip a	0.35	10.9	0.61	3.48	5.63	18.8885	15.5864	38.9612	19	
				” b	0.54	14.2	0.40	3.00	2.97	18.8937	15.5870	38.9694	20	
				” c	0.38	14.0	0.80	3.75	5.17	18.8850	15.5845	38.9523	22	
				” d	0.44	15.6	0.66	2.94	6.19	18.8871	15.5834	38.9534	12	
				” e	0.24	10.2	0.53	4.17	7.62	18.8890	15.5828	38.9540	20	

Sample name	Eruption date	Sample type		$EF^{(3)}_{(Ni)}$	$EF_{(Cu)}$	$EF_{(Tl)}$	$EF_{(Pb)}$	$EF_{(Bi)}$	$^{206}Pb/^{204}Pb$ $(\pm2\sigma)^{(2)}$	$^{207}Pb/^{204}Pb$ $(\pm2\sigma)^{(2)}$	$^{208}Pb/^{204}Pb$ $(\pm2\sigma)^{(2)}$	ng Pb$^{(1)}$	Blank correction$^{(2)}$ (%)
			Crushed chip	a 7.82	27.6	0.45	1.94	2.70	18.8327	15.5829	38.8794	5.2	
			”	b 7.69	27.2	0.40	1.97	3.24	18.8336	15.5835	38.8829	5.7	
150212-13	Feb-15	Glassy lapilli	Crushed chip	a 0.52	8.22	35.3	5.17	9.13	18.8666	15.5887	38.9392	20	
			”	b 0.51	7.81	33.8	5.10	9.32	18.8646	15.5899	38.9425	23	
			”	c 0.49	8.10	35.5	5.29	8.24	18.8638	15.5893	38.9413	22	
150212-16	Feb-15	Glassy lapilli	Crushed chip	0.37	2.07	4.11	3.17	65.8	18.8728	15.5963	38.9671	3.5	

Pb isotopic compositions are relative to NBS 981 values: $^{206}Pb/^{204}Pb = 16.9356$, $^{207}Pb/^{204}Pb = 15.4891$, $^{208}Pb/^{204}Pb = 36.7006$ (1) amount of Pb extracted (2) in-run internal error and blank correction for samples with less than 0.3 ng Pb (3) EF: Enrichment Factor relative to Ce (see text for details).

(40–60 μm) spherules with 63–72 wt.% Fe (Fig. 1c) were found while picking the magnetic fraction (e.g., in sample 1012-136), but were not observed *in-situ* in these recent samples.

3.2. Trace element and Pb isotope analysis

3.2.1. Iron oxide globules (PDN17)

The two batches of globules analyzed have 1.16–1.29 wt.% Cu, 0.41–0.55 wt.% Mn, 0.19–0.53 wt.% Ti, 0.29–0.32 wt.% Zn, 325–345 ppm Co, 364–421 ppm Ni, 36–140 ppm Bi, 40–48 ppm Li, 12–47 ppm Ba, 32–74 ppm La, and 2.9–8.5 ppm Pb. Compared to the host rock, Bi and Cu are enriched by a factor of 10^3, Zn, Ni, Li, and As are enriched by a factor of 10–30, while Ti, Nb, Ba, Th, and Zr are depleted by a factor of 3–10 (Fig. 2a). Assuming that all Zr (16–38 ppm) originates from the silicate fraction attached to the globules (with 152 ppm Zr according to PDN17 whole rock analysis) allows us to estimate the silicate mass fraction to be in the range of 10–25%. The Cu/Ni ratio (27.5–35.5) is an order of magnitude higher than in the host rock (3.74). Note that the host rock ratio is already three times higher than in less differentiated samples (1.5 ± 0.1), mainly because of Ni depletion. The $^{206}Pb/^{204}Pb$ and $^{208}Pb/^{204}Pb$ of the two globule samples are identical within error, with an average of 18.375 and 38.407, respectively. These ratios are much lower than in the host rock (18.824 and 38.942). They are also less radiogenic than the least radiogenic ratios (18.654 and 38.709) measured in La Réunion sub-aerial lavas to date (Oversby, 1972; Bosch et al., 2008). Conversely, the $^{207}Pb/^{204}Pb$ ratio of the globules (average of 15.603) is similar to that of host rock (15.591).

3.2.2. Magnetic fractions

Compared to their host rocks, the magnetic separates from the recent pumice samples (1406-24-3; 141118-3, 150212-13 and 1012-136) are enriched in Cu, Ni and Bi by a factor of 4–8 on average, and of up to 10–20 in sample 1012-136 (Fig. 2a). Cu and Ni concentrations tightly correlate (Fig. 3a). The Cu/Ni ratio (2.2 ± 0.4) is intermediate between bulk rocks (1.5 ± 0.1) and sulfides from the Bellecombe Ash deposit (2.9 ± 1.8, excluding one value at 0.7) (Upton et al., 2000). By comparison, the average Cu/Ni ratios of primary melt inclusions and matrix glasses are 1.5 and 2.5, respectively (Di Muro et al., 2014). No significant enrichment in other elements is detected. The magnetic fraction is more important in the dense spatter samples (140624-13a, 141118-5-d, 141118-5-l) than in pumices (2.0–7.3 mg for dense spatter against 0.06–3.0 mg for pumice) due to the abundance of magnetite microlites that probably formed during lava cooling. No Cu–Ni enrichment is detected in the dense spatter magnetic fraction.

All four separates enriched in Cu-Ni show Pb isotope disequilibria relative to the host rocks (Fig. 3bc); three samples have lower $^{206}Pb/^{204}Pb$ and $^{208}Pb/^{204}Pb$ ratios. The isotopic shift is small (ca. 700 ppm) but remains clearly outside analytical error. These three samples plot on the same trend of decreasing $^{206}Pb/^{204}Pb$ and $^{208}Pb/^{204}Pb$ ratios with increasing Cu concentration as the globules of PDN17.

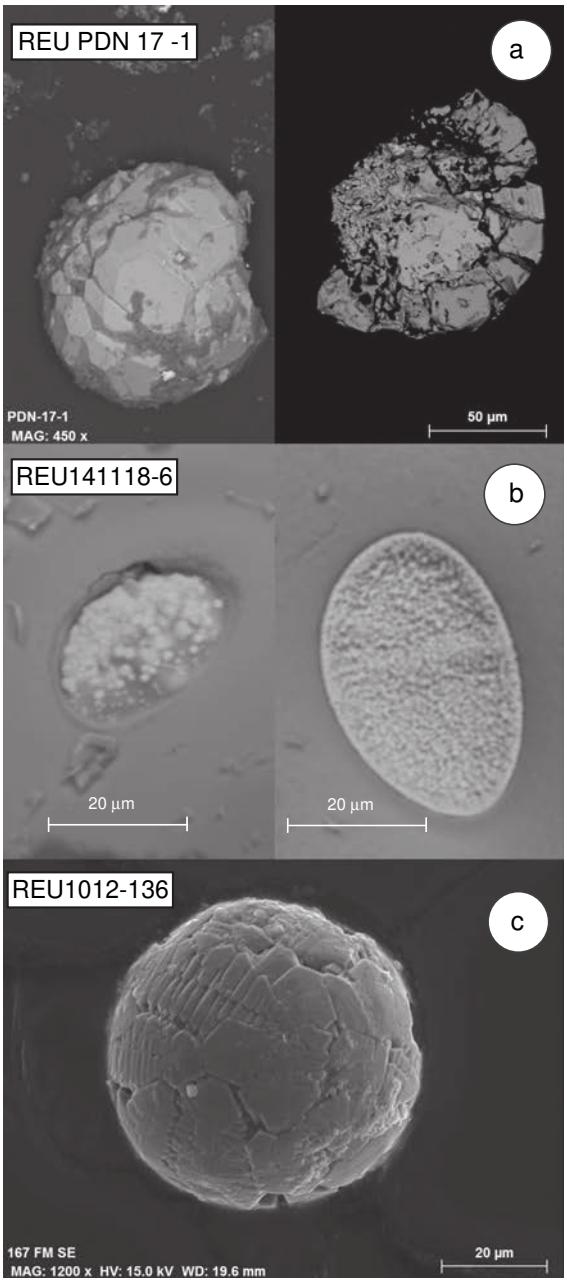

Fig. 1. Scanning Electron Microscopy (SEM) imaging of the Fe–Cu oxides in Backscattered Electron (BSE) mode. (a) Globule n°1 from sample PDN17 (Piton des Neiges). Right panel: Polished section of the same globule. Compositional zoning reflects Cu enrichment (3–5%) of the outer shell. (b) Fe–Cu oxide coatings within vesicles of a recent pumice sample from Piton de la Fournaise (sample 141118-6 from the June 2014 eruption). (c) Spherule with 63–72 wt.% Fe found in the magnetic fraction of a glassy pumice (sample 1012-136 from the December 2010 eruption). BSE images and EDS compositions of all studied samples are reported in Supplementary Table A.

The picture is less clear for $^{207}Pb/^{204}Pb$, as only two of the three samples have distinctly low ratios (not shown). Conversely, the fourth sample (1012-136), which shows the highest Cu–Ni enrichment, has a much more radiogenic Pb isotopic composition ($^{206}Pb/^{204}Pb = 19.454$, $^{207}Pb/^{204}Pb = 15.655$, $^{208}Pb/^{204}Pb = 39.021$) than the host rock. Its $^{206}Pb/^{204}Pb$ ratio is also the highest of all La Réunion rocks analyzed to date ($^{206}Pb/^{204}Pb < 19.1$).

3.2.3. Leachates

Element enrichment in leachates is investigated through the use of elemental enrichment factors (EF_x), defined as:

$$EF_x = \frac{\left(\frac{E_x}{E_r}\right)_{\text{leachate}}}{\left(\frac{E_x}{E_r}\right)_{\text{lava}}} \quad (1)$$

where E_r is the concentration of reference element r. Cerium is used as the reference element because it is lithophile and relatively fluid mobile (in order to correct for the effect of silicate leaching) but not chalcophile. Cerium is also amongst the less volatile elements at Piton de la Fournaise (Vlastélic et al., 2013). Elements commonly enriched in leachates include Pb ($0.93 < EF_{Pb} < 5.7$), Li ($0.97 < EF_{Li} < 14.1$), as ($0.97 < EF_{As} < 14.7$), Cu ($1.1 < EF_{Cu} < 29.5$), Bi ($0.9 < EF_{Bi} < 64$) (Fig. 2b). Thallium can be either very enriched or depleted ($0.46 < EF_{Tl} < 162$). Nickel is generally depleted ($0.3 < EF_{Ni} < 1.3$) except in the interior of sample 141118-6 (EF_{Ni} of 8.9), which also shows the highest Cu enrichment ($EF_{Cu} = 29.5$) and significant enrichment in Mn ($EF_{Mn} = 7$), Co ($EF_{Co} = 5.1$), Zn ($EF_{Zn} = 3.6$), and Cd ($EF_{Cd} = 3.5$) (Fig. 2b). Interestingly, this sample was collected at the base of the June 2014 lapilli fallout bed, which was produced at the beginning of the eruption when the magma eruption rate was the highest. Element fraction unsupported by silicate input is defined as:

$$E_{x(\text{Si unsupported})} = 1 - \frac{1}{EF_x}, \quad (2)$$

which allows us to estimate that up to 82%, 89%, 97% and 98% of the Pb, Ni, Cu and Bi budget of leachates originate from non silicate phases, respectively. However, these numbers should be considered with caution, as they do not account for fractionation between mobile and less mobile elements during leaching.

The $^{206}Pb/^{204}Pb$ and $^{208}Pb/^{204}Pb$ ratios of leachates extend from values within the ranges of whole-rocks (18.899–18.905 and 38.986–39.003, respectively) to significantly lower values (down to 18.833 and 38.879, respectively). Remarkably, the $^{206}Pb/^{204}Pb$ and $^{208}Pb/^{204}Pb$ ratios negatively correlate with Cu enrichment (i.e., EF_{Cu} or E_{Cu}; Fig. 4). This relation also holds within individual samples (1001-053 and 140624-3). Such a relation between Cu enrichment and Pb isotopes has been previously identified in samples from 1977 and 2001–2003 eruptions (Vlastélic and Staudacher, 2014), suggesting it is a common feature of fresh lavas from La Réunion. Lead isotope ratios also negatively correlate with Pb enrichment (i.e., EF_{Pb} or E_{Pb}), but the relation is less clear than for Cu, probably due to lower Pb enrichments. Note also that the leachates of uncrushed samples (i.e., leaching of scoria outer surface) are enriched in Cu but the Pb isotopic disequilibrium is less than for crushed samples. The $^{207}Pb/^{204}Pb$ variations (15.583–15.601) encompass those of whole rocks (15.591–15.597), but the correlation with Cu is less clear.

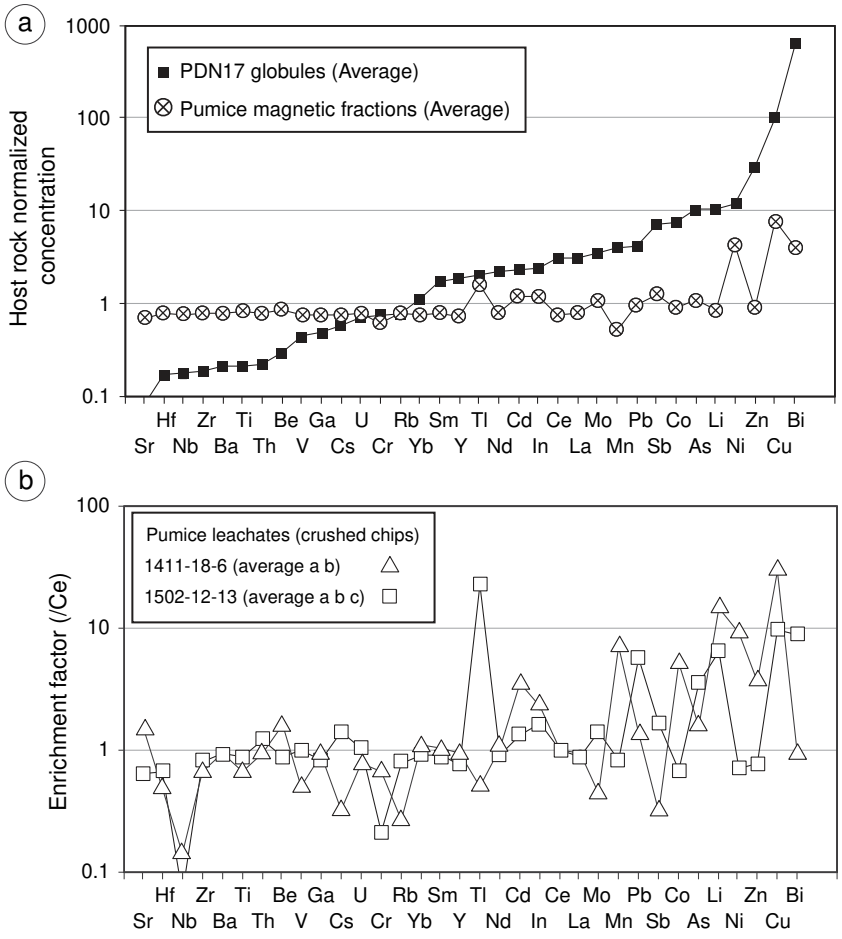

Fig. 2. Fe oxide trace element patterns. (a) Host rock normalized concentrations. Trace element patterns are shown for PDN17 globules (average of batch A and B) and the magnetic fractions of pumice samples (average of samples 1406-24-3, 141118-3, 150212-13, and 1012-136). Elements are ordered from left to right according to their enrichment in PDN17 globules. (b) Element enrichment factors (EF) in the acid leachates of crushed chips of pumices. Cerium is used as the reference element (see text for details). Average trace element patterns are shown for samples showing the highest Cu enrichment (1411-18-6 and 1502-12-13 with EF_{Cu} of 29.3 and 9.6, respectively). Trace element data of the Fe oxide separates (PDN17 globules, magnetic fractions and acid leachates) and host rocks are reported in Supplementary Tables B and C, respectively.

Only samples with $EF_{Cu} > 10$ have distinctly lower $^{207}Pb/^{204}Pb$ (Fig. 4b).

Although the lead isotope compositions of the leachates are generally less radiogenic than in the host lavas, the compositions remain within the isotopic range of lavas erupted at Piton de la Fournaise since 0.5 Ma (Bosch et al., 2008). Moreover, most compositions are within the range of historical lavas (1927–2007).

4. DISCUSSION

4.1. Evidence for sulfide entrainment and destabilization

The Fe oxides hosted in La Réunion rocks meet several textural and chemical criteria aimed at distinguishing sulfide breakdown products from magnetite crystallizing from silicate melt (Larocque et al., 2000): (1) globular shape, (2) large size compared to magmatic sulfides, (3) similar occurrence as sulfides (e.g., in drastically quenched samples) (4) core-rim compositional and textural zonation (spongy, Cu-rich rim), (5) absence of Ti, and (6) presence of Cu and Ni. In addition, the Pb isotope disequilibrium between Fe oxides and their host rocks is best explained by the destabilization of genetically unrelated sulfides that were assimilated by La Réunion plume melts as they rose through the oceanic lithosphere and crust.

Remnants of sulfide liquids have been reported in quenched magmas from arc volcanoes, including Pinatubo (Philippines) and Mt. St. Helens (USA), Popocatepetl (Mexico), and Satsuma-Iwojima (Japan; Larocque et al., 2008, 2000; Di Muro et al., 2008). Coatings of Fe–Cu oxides were also found to occur in vesicles of quenched samples from Kilauea volcano, Hawaii (Strand et al., 2002), but were not formally ascribed to sulfide destabilization.

Main factors controlling sulfide breakdown include (1) the abrupt increase of sulfur content at sulfur saturation between FMQ and FMQ+2 (Jugo, 2009), (2) increasing sulfur solubility with increasing FeO content of the melt

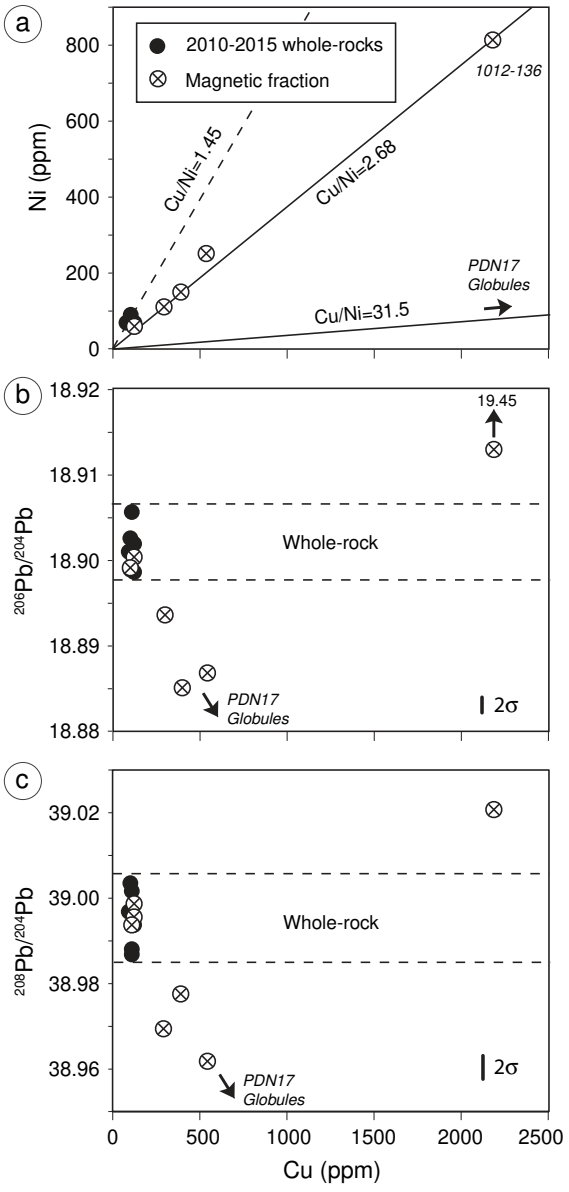

Fig. 3. Cu–Ni and Pb isotope signatures of the magnetic separates. (a) Ni versus Cu concentration. (b) ($^{206}Pb/^{204}Pb$) versus Cu concentration. (c) ($^{208}Pb/^{204}Pb$) versus Cu concentration. Host rock compositions are shown for comparison (whole–rock data from Supplementary Table C). External precision (2σ) of Pb isotope measurements is indicated. Arrows indicate data points that lie beyond the scale of the plot.

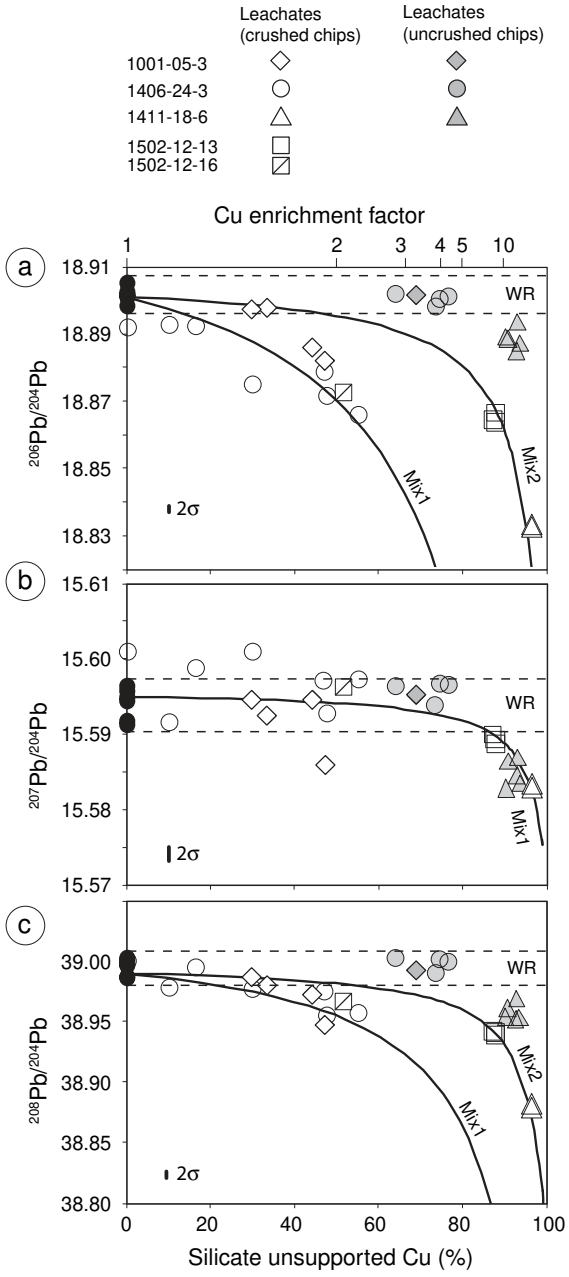

Fig. 4. Lead isotope composition versus Cu enrichment in leachates. Whole–rock compositions (black circles) are shown for comparison (Supplementary Table C). Cu enrichment factor and silicate unsupported Cu (in%) are defined in the text. External precision (2σ) of Pb isotope measurements is indicated. Mixing curves between silicate melt (1.6 ppm Pb, 44 ppm Ce, 109 ppm Cu, $^{206}Pb/^{204}Pb = 18.90$, $^{207}Pb/^{204}Pb = 15.595$, $^{208}Pb/^{204}Pb = 38.99$) and Fe–Cu oxide with a composition similar to PDN17 globules (8 ppm Pb, 65 ppm Ce, 1.2% Cu) are shown. The compositional variation of leachates (crushed chips) requires the Fe–Cu oxide end-member composition to range between MIX 1 ($^{206}Pb/^{204}Pb = 18.20$, $^{207}Pb/^{204}Pb = 15.575$, $^{208}Pb/^{204}Pb = 38.20$) and MIX 2 ($^{206}Pb/^{204}Pb = 18.77$, $^{207}Pb/^{204}Pb = 15.575$, $^{208}Pb/^{204}Pb = 38.80$).

(O'Neill and Mavrogenes, 2002), which occurs, for instance, during plagioclase crystallization (Mathez, 1976), and (3) low pressure sulfur degassing in response to decreasing sulfur solubility in silicate melts below 100 MPa (Lesne et al., 2011). The process of sulfide breakdown has been discussed only in subduction zone settings (Larocque et al., 1998, 2000; Nadeau et al., 2010, 2013; Di Muro et al., 2008; Berlo et al., 2014): scenarios involving S_2 loss followed by S_2 oxidation, reaction of sulfide with H_2O dissolved in the melt, or reaction of sulfides with a magmatic volatile phase have been proposed. Here we emphasize that the process of sulfide breakdown will depend on the timing of oxidation relative to that of S

degassing. The two processes are tightly linked in a complex manner, however (Mathez, 1984; Burgisser and Scaillet, 2007). If oxidation occurs before S degassing, for instance through degassing of the less soluble C species (Mathez, 1984), or input of H_2O-rich fluids, sulfide dissolution might occur; such a situation might dominate in subduction zone settings. Conversely, in the case of sub-aerial intraplate volcanism, oxidation from FMQ-2 to FMQ+1 occurs late during the eruption and emplacement of lavas (Rhodes and Vollinger, 2005; Boivin and Bachèlery, 2009), when S solubility is very low (a few hundreds of ppm at most). In such a situation, sulfide might not dissolve into the melt, but destabilize with direct transfer of S and chalcophile elements to the gas phase. The occurrence of thin Fe–Cu oxide coatings on vesicles walls indeed suggests that, in some circumstances, elements were last transported in a vapor phase. The spiky outgrowths of PDN17 globules are also consistent with condensation of magmatic vapor trapped in vesicles. However, volatile chloride compounds, whose role in metal transport is well established (e.g., Strand et al., 2002), were not detected in our samples.

Upward transfer of sulfide liquids is consistent with the observation that magma ascent velocities at La Réunion are high enough to entrain olivine crystals typically 5 mm in size (and up to several cm), producing the so called "oceanite" eruptions comprising up to 60% of cumulative olivine. The settling velocity of a spherical particle (sulfide or olivine) in a silicate melt can be estimated from the Stokes law (Holzheid, 2010):

$$V_{\text{particle}} = \frac{g \cdot d^2 \cdot (\rho_{\text{particle}} - \rho_{\text{silicate}})}{18 \cdot \eta_{\text{silicate}}} \quad (3)$$

where g is the gravity constant, d is the diameter of the particle, ρ is density, and η is viscosity. The size ratio between sulfide and olivine with identical settling velocities is:

$$\frac{d_{\text{sulfide}}}{d_{\text{olivine}}} = \sqrt{\frac{\rho_{\text{olivine}} - \rho_{\text{silicate}}}{\rho_{\text{sulfide}} - \rho_{\text{silicate}}}} \quad (4)$$

Taking densities of 2700, 3320 and 3750–4900 kg/m^3 for silicate melt, olivine and sulfide, respectively, it is estimated that entrained sulfides are only 0.77–0.53 times smaller than entrained olivine crystals. This indicates that millimeter size sulfides can potentially be transported upward during high flux eruptions. According to Eq. (3), the size of entrained sulfides decreases by a factor of two during normal eruptions, with eruption rates typically four times lower than during high flux eruptions, and assuming a four times lower magma ascent velocity. These observations strongly suggest that sulfide droplets such as those found in the interstitial glass of Bellecombe cumulates (<40 μm) are efficiently transferred upward by rising magmas, without necessarily being attached to gas bubbles (Mungall et al., 2015).

4.2. Lead isotope constrains on the origin of the Fe–Cu oxides

Although the issue of contamination was considered with great care, the possibility of the addition of foreign Pb, either *in-situ* after eruption or in the laboratory, must be evaluated before using Pb isotope data to constrain the origin of the iron-oxide parental sulfides. First, we emphasize that all samples except PDN17 were collected during eruption, or shortly after. Loss on ignition is systematically negative (from −0.9 to −0.3) due to Fe oxidation, which indicates that samples have not equilibrated with the air. The occurrence of Fe–Cu oxides in the vesicles of spatters collected during eruption indicates that the oxides are syn-eruptive phases, unambiguously indicating that the iron oxides cannot result from post-eruption circulation of hydrothermal fluids. Although sample PDN17 was collected 230–350 ka after eruption, several observations suggest that PDN17 Fe–Cu oxide globules have a magmatic rather than a hydrothermal origin: (1) a complete inventory of amygdale minerals at Piton des Neiges identified 36 species, including zeolites, calcite, aragonite, pyrite, quartz, and albite, but not iron oxide (Rançon, 1985). (2) The globules are depleted in mobile elements commonly found in hydrothermal fluids, such as Sr and Ba, but are enriched in volatile elements and Ni (Fig. 2a). (3) The Pb isotope signature of hydrothermal fluids is expected to be a mixture between basalt derived Pb and pre-anthropogenic seawater/atmospheric Pb, the composition of which is best recorded in deep sea Fe–Mn deposits (Vlastélic et al., 2001). As shown in Fig. 5, PDN17 globules do not plot on a mixing line (i.e., a straight line in Pb–Pb isotope space) between La Réunion basalts and seawater/atmospheric Pb. (4) As noted in the results section, PDN17 globules are very similar in composition to the Fe oxides found in lavas collected during the recent eruptions of Piton de la Fournaise volcano.

Contamination during sample handling and Pb extraction has been rigorously evaluated by repeatedly measuring both the blank amount and isotopic composition. Blank contribution is negligible for 33 out of 36 samples, and is corrected for in the three instances.

The possibility that Pb isotope data are biased due to contamination in the laboratory can be ruled out for several reasons: (1) there is no simple relationship between the amount of Pb extracted and the Pb isotopic composition. (2) Irrespective of blank correction, the Pb composition of the smallest sample (1012-136 with 74 pg Pb) is more radiogenic than the host rock, whereas all measured blanks are less radiogenic. Such a signature is ascribed to the presence of a magnetite spherule is this sample. (3) Although some of the smallest samples (PDN17 globules) have $^{207}Pb/^{204}Pb$ and $^{206}Pb/^{204}Pb$ ratios similar to the blank, their $^{208}Pb/^{204}Pb$ (>38.40) are significantly higher than the blank value (38.005 ± 0.174; Fig. 5). Accounting for the maximum uncertainties on blank amount and composition would not introduce an overlap in the $^{208}Pb/^{204}Pb$ data. (4) Overall, no sample plots on a mixing line between basalt and blank compositions in three-dimensional Pb isotope space (Fig. 5).

Altogether, these arguments indicate that the reported Pb isotope compositions represent the primary signature of the Fe–Cu oxides, allowing us to address the origin of the Pb and the process by which it is incorporated into the Fe oxides. Since a large fraction of Pb initially present in sulfide partitions into the fluid and gas phases (Berlo et al., 2014), it is uncertain whether Pb hosted in the Fe oxides is truly residual, or has been partitioned into the gas

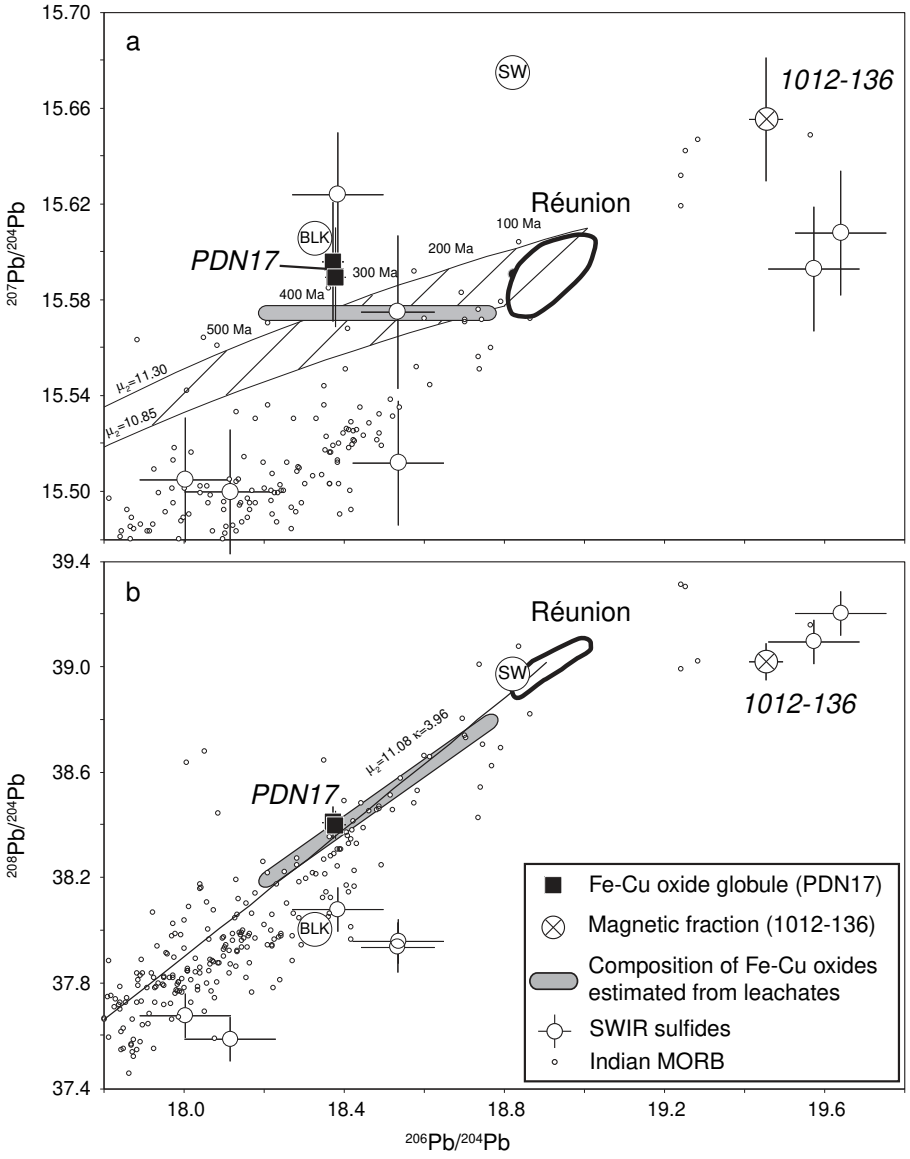

Fig. 5. Pb–Pb isotope plots. (a) $^{207}Pb/^{204}Pb$ vs. $^{206}Pb/^{204}Pb$. (b) $^{208}Pb/^{204}Pb$ vs. $^{206}Pb/^{204}Pb$. The composition of PDN17 globules (black squares) and magnetic fraction of sample 1012-136 (circle with a cross) are compared to the signature of La Réunion rocks (''Réunion'' labeled field). The gray field indicates the composition of the parental sulfides of the Fe–Cu oxides estimated from leachates (Fig. 4). The compositions of the procedural blank (BLK) and regional seawater (SW; Vlastélic et al., 2001) are reported. The composition of Indian Mid-Ocean Ridge Basalts (MPI GEOROC database, http://georoc.mpch-mainz.gwdg.de/georoc/) and sulfides from the Southwest Indian ridge (SWIR) peridotites (Warren and Shirey, 2012) are shown. Lead isotope growth curves starting from the composition of the Canyon Diablo meteorite and ending at the present day La Réunion composition are shown, assuming $^{238}U/^{204}Pb$ (μ) increased from 7.93 to 10.85–11.30 2.43 Ga ago (secondary isochron age inferred from the $^{207}Pb/^{204}Pb$ vs. $^{206}Pb/^{204}Pb$ slope shown by La Réunion data). (a) Ages before present are indicated along the isotope growth curves. In (b), the growth curve is shown for a $^{232}Th/^{238}U$ (k) abundance ratio of 3.96.

phase and subsequently condensed. In the latter case, addition of gaseous Pb from foreign sources cannot be ruled out. At Vulcano Island (Italy), occasional contamination of volcanic gas with atmospheric lead occurs when seismic or tectonic events modify edifice permeability (Nonell et al., 2005). Atmospheric aerosols collected upwind of La Réunion Island in 2007 have $^{207}Pb/^{206}Pb$ and $^{208}Pb/^{206}Pb$ ratios in the range of 0.842–0.849 and 2.057–2.071, respectively (Witt et al., 2010). Although these values are within the range of the Fe oxides (0.805–0.849 and 2.006–2.049), they plot well off the Fe oxides array (not shown) suggesting that atmospheric aerosols scavenged by rainwater are not the source of Pb hosted in the Fe oxides. In support of this conclusion, the impervious shell surrounding the magma chamber of Piton de la Fournaise prevents meteoritic water-magma interaction (Violette et al., 1997).

In keeping with the arguments developed in Section 4.1, it is suggested that Pb hosted in the Fe oxides originates from magmatic sulfides, either directly or via an intermediate gas phase. The relationship between Cu enrichment and

Pb isotopic composition in the leachates of La Réunion samples (Fig. 4) allows us to estimate the composition of parental sulfides to be $^{206}Pb/^{204}Pb = 18.20–18.77$, $^{207}Pb/^{204}Pb = 15.575$ and $^{208}Pb/^{204}Pb = 38.2–38.8$, which is consistent, within error, with the more direct measurements made on the Fe–O–Cu globules of sample PDN17. This composition is less radiogenic than most La Réunion lavas (>95% of La Réunion samples analyzed to date have $^{206}Pb/^{204}Pb > 18.80$) (Fig. 5). Assuming that sulfides were in isotopic equilibrium with La Réunion magmas at the time of formation (i.e., they exsolved from ancient plume melts), and that they froze radiogenic Pb ingrowth (i.e. $U/Pb \sim 0$), between 100 and 400 Ma is needed to develop the unradiogenic Pb signature estimated for the Fe oxide parental sulfides. This age is much older than the maximum age of 8 Ma estimated for the La Réunion edifice (Charvis et al., 1999), ruling out the remobilization of sulfides exsolved during the early stage of La Réunion magmatism.

A key observation is that the Pb isotopic compositions of the Fe–Cu oxides are either less or more radiogenic than host rocks, although the first case is far more frequent (all but one sample). Similar Pb isotope disequilibrium exists between sulfides and host abyssal peridotites, where the dominant unradiogenic Pb signature is ascribed to an ultra-refractory, under-sampled upper mantle reservoir (Burton et al., 2012; Warren and Shirey, 2012; Blusztajn et al., 2013). Hart and Gaetani (2006) suggested that plume melts are likely under-saturated in sulfide and tend to assimilate or equilibrate with genetically unrelated sulfides from the lithosphere or crust. Comparing the composition estimated for the parental sulfides of the Fe oxides to that of sulfides from the Southwest Indian ridge (SWIR) peridotites (Warren and Shirey, 2012) reveals some resemblance in $^{207}Pb/^{204}Pb$ vs. $^{206}Pb/^{204}Pb$ space, but the composition estimated for La Réunion sulfides is higher in $^{208}Pb/^{204}Pb$ at a given $^{206}Pb/^{204}Pb$ than SWIR sulfides (Fig. 5). It is unlikely that this shift reflects an inter laboratory bias since both data sets are normalized to the same NBS981 values of Todt et al. (1996). Conversely, the radiogenic Pb composition of sample 1012-136 plots near the radiogenic SWIR sulfides in $^{208}Pb/^{204}Pb$ vs. $^{206}Pb/^{204}Pb$ space, but slightly above in $^{207}Pb/^{204}Pb$ vs. $^{206}Pb/^{204}Pb$ space (Fig. 5). Thus, any genetic relation between La Réunion sulfides and nearby abyssal peridotite sulfides is not obvious. However, the composition estimated for La Réunion sulfides does plot within the field of Indian MORB, raising the possibility that La Réunion melts assimilate or equilibrate with sulfides from the Indian Ocean crust.

4.3. Implication for SO_2 degassing

Because sulfides are roughly one third S, they are expected to play an important role in the total sulfur budget of intraplate basaltic magmas with low amounts of dissolved sulfur (ca. 1400 ppm at FMQ; Jugo et al., 2005). Whether immiscible sulfide liquids sink or are transferred upward will strongly influence SO_2 degassing. Yet, the general good agreement between the amount of sulfur in volcanic plumes and that predicted from S abundance in melt inclusions (Sharma et al., 2004) suggests either that sulfides existing at the time of melt inclusion entrapment are not transferred upward, or that sulfides play a minor role in the sulfur budget.

Based on Cu depletion in La Réunion differentiated lavas, Collins et al. (2012) estimated a sulfide mass fraction in the range of 0.1 to 0.5% which represents between 19% and 93% of the sulfur budget (taking as reference 1740 ppm S). Similarly, constraints on sulfide mass fraction may be obtained from Pb isotope mass balance. The effect of adding sulfide with $^{206}Pb/^{204}Pb$ ratio of 18.50 (median value estimated for Fe–Cu oxide parental sulfides) to silicate melt with $^{206}Pb/^{204}Pb$ ratio of 18.905 (baseline composition of recent lavas from Piton de la Fournaise; Vlastélic et al., 2009) is evaluated using Pb partition coefficients between sulfide liquid and silicate melt ($D_{Pb}^{SL/SM}$) ranging from 24 to 66 (Li and Audétat, 2015; Hart and Gaetani, 2016). The mixture composition is compared to short-term variations in bulk rock Pb isotope composition (Fig. 6), whose lack of correlation with source tracers involving lithophile elements (e.g. $^{87}Sr/^{86}Sr$ or La/Sm) has been ascribed to contamination of the La Réunion plume melts by foreign sulfides from the oceanic lithosphere or crust (Vlastélic et al., 2009). The least radiogenic $^{206}Pb/^{204}Pb$ ratios of lavas (18.86) can be explained by addition of 0.19 ($D_{Pb}^{SL/SM} = 66$) to 0.52 ($D_{Pb}^{SL/SM} = 24$) wt.% sulfides, which agrees well with the previous estimate of

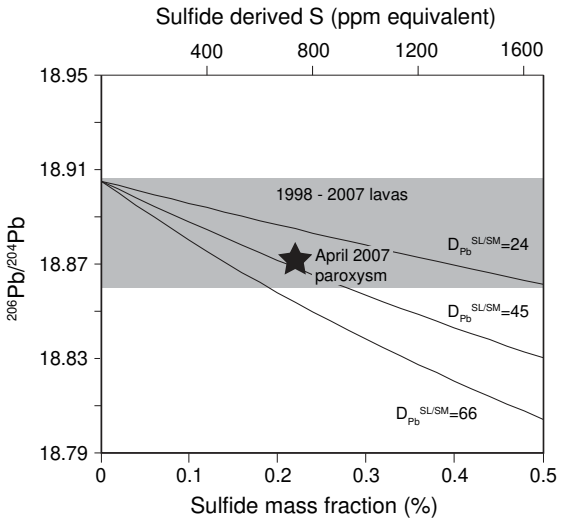

Fig. 6. Relation between Pb isotopic composition and sulfide mass fraction. Mixing curves between silicate melt with $^{206}Pb/^{204}Pb = 18.905$ (baseline composition of recent lavas from Piton de la Fournaise; Vlastélic et al., 2009) and sulfide with $^{206}Pb/^{204}Pb = 18.50$ (median value estimated for Fe–Cu oxide parental sulfides) are shown for Pb partition coefficients between sulfide liquid and silicate melt ($D_{Pb}^{SL/SM}$) ranging from 24 to 66 (Li and Audétat, 2015; Hart and Gaetani, 2016)). Gray field: short-term (1998–2007) variations in bulk rock Pb isotope composition (Vlastélic et al., 2009). Star: estimated composition for the April 2007 eruption paroxysm assuming sulfide destabilization accounts for the excess SO_2 emissions (see text). Upper x axis: amount of S delivered by sulfide breakdown (assuming 33.5 wt% S in sulfide). This amount should be compared to the ca. 1100 ppm dissolved S in pre-eruptive magmas (Di Muro et al., 2014).

Collins et al. (2012). However, in contrast with previous inferences, our results suggest (1) addition of genetically unrelated sulfides, and (2) upward transfer and late stage degassing of sulfides.

Sulfide degassing will yield excess SO_2 emissions compared to the amount predicted based on dissolved sulfur alone. The eruption of April 2007, the most voluminous of the last century, is well suited to address this issue because SO_2 emissions, magma flux, and the sulfur content of pre-eruptive magmas are well documented (Tulet and Villeneuve, 2011; Gouhier and Coppola, 2011; Coppola et al., 2009; Collins et al., 2012; Di Muro et al., 2014). Considering the sulfur content of pre-eruptive magmas (1100 ppm), the residual sulfur content in degassed lavas (200 ppm), and the magma discharge rate (200 m^3/s), we estimate that the SO_2 emission rate (1800 kg/s) exceeds the degassing rate of dissolved sulfur (1007 kg/s SO_2) by a factor of 1.8 during the paroxysmal phase (6 April). Note that a greater sulfur excess (a factor of 2.6) has been estimated for the 6–13 April period (Gouhier and Coppola, 2011), so our estimate should be considered a minimum value. Such excess S emissions have been ascribed to the opening of a hydrothermal system during summit collapse (Gouhier and Coppola, 2011), or degassing of un-erupted deep magmas (Di Muro et al., 2014). The unradiogenic Pb anomaly ($^{206}Pb/^{204}Pb = 18.87$) of lavas erupted during the paroxysmal phase (Vlastélic et al., 2009) suggests that the excess SO_2 emissions originate from entrainment and destabilization of foreign sulfides. We estimate that 0.22 wt.% sulfides (equivalent to 720 ppm dissolved S) is needed to explain the 80% SO_2 excess observed on April 6 (Fig. 6). This sulfide fraction is consistent with the Pb isotope mixing model (Fig. 6), the composition estimated for the parent sulfides ($^{206}Pb/^{204}Pb = 18.50$), and $D_{Pb}^{SL/SM} = 45$, within the range of recently published values (Li and Audétat, 2015; Hart and Gaetani, 2016). We suggest that sulfide addition (and saturation) and destabilization are not recorded in the S content of 2007 melt inclusions because these events occur deeper (>300 Mpa) and shallower (near or at the surface), respectively, than the level of melt inclusion entrapment (10–50 MPa; Di Muro et al., 2014). Note that the sulfur budget described above is based on syn-eruptive SO_2 emissions, and does not take into account the weak, but prolonged (>2 years) degassing of the thick (up to 60 m) 2007 lava flow. Fumarolic incrustations (sulfates and fluorides) that formed between one and three years after the eruption at temperatures between 400 and 100 °C display unradiogenic Pb and Os isotope signatures that indicate a sulfide contribution of 0.004–0.06% to magmatic fluids (Vlastélic et al., 2013; Gannoun et al., 2015). Thus, sulfide breakdown might also occur during the progressive oxidation of lava flow interiors, and contribute to late SO_2 degassing.

5. CONCLUSIONS

Iron oxide globules and coatings were found to occur in vesicles of differentiated lavas from Piton des Neiges and recent pumice samples from Piton de la Fournaise. The Fe oxides do not contain sulfur, but are enriched in Cu (±Ni) and other chalcophile elements (e.g. Bi) compared to the host lavas. Systematic Pb isotope disequilibrium (between 500 ppm and 2.9% for $^{206}Pb/^{204}Pb$) exists between Fe oxides and their host rocks. The occurrence pattern, texture, and chemical and isotopic composition of the Fe–Cu oxides hosted in La Réunion rocks strongly suggest that they are products of the oxidation and devolatilization of an immiscible sulfide liquid. These findings have the following implications:

(1) Despite their high density, sulfides are probably transferred upward during eruptions. It is estimated that magma ascent velocities at Piton de la Fournaise are sufficient to counterbalance the settling velocities of millimeter-size sulfides.
(2) In most cases, the Pb isotope disequilibrium between Fe oxides and their host rocks is too large to be explained by the remobilization and destabilization of ancient co-genetic sulfides. Instead, the Fe oxide parent sulfides most likely originate from the local oceanic lithosphere or crust.
(3) These foreign sulfides contribute to SO_2 degassing, which may explain some of the inconsistency between measured SO_2 emissions and those predicted from the S content of melt inclusions.

ACKNOWLEDGEMENTS

This work benefited from the financial support from the Agence Nationale de la Recherche (DEGAZMAG project, contract no. ANR 2011 Blanc SIMI 5-6 003), the French Government Laboratory of Excellence initiative n°ANR-10-LABX-0006, the Région Auvergne and the European Regional Development Funds. We thank the anonymous reviewers and the editors, W. Sun (AE) and M. Norman (EE), for their constructive comments and for handling the manuscript. Thanks to R. Dennen (RD Editing Services) for English editing. This is Laboratory of Excellence ClerVolc contribution number 215.

APPENDIX A. SUPPLEMENTARY DATA

Supplementary data associated with this article can be found, in the online version, at http://dx.doi.org/10.1016/j.gca.2016.08.036.

REFERENCES

Berlo K., van Hinsberg V. J., Vigouroux N., Gagnon J. E. and Williams-Jones A. E. (2014) Sulfide breakdown controls metal signature in volcanic gas at Kawah Ijen. *Chem. Geol.* **371**, 115–127.

Blusztajn J., Shimizu N., Warren J. M. and Dick H. J. B. (2013) In-situ Pb isotopic analysis of sulfides in abyssal peridotites: New insights into heterogeneity and evolution of the oceanic upper mantle. *Geology*. http://dx.doi.org/10.1130/G3496.1.

Boivin P. and Bachèlery P. (2009) Petrology of 1977 to 1998 eruptions of Piton de la Fournaise, La Réunion Island. *J. Volcanol. Geotherm. Res.* **184**, 105–109.

Bosch D., Blichert-Toft J., Moynier F., Nelson B. K., Télouk P., Gillot P.-Y. and Albarède F. (2008) Pb, Hf and Nd isotope compositions of the two Réunion volcanoes (Indian Ocean): a

tale of two small-scale mantle "blobs"? *Earth Planet. Sci. Lett.* **265**, 748–768.

Burgisser A. and Scaillet B. (2007) Redox evolution of a degassing magma rising to the surface. *Nature* **445**, 194–197.

Burton K. W., Cenki-Tok B., Mokadem F., Harvey J., Gannoun A., Alard O. and Parkinson I. J. (2012) Unradiogenic Pb in Earth's upper mantle. *Nat. Geosci.* **5**, 570–573.

Charvis P., Laesanpura A., Gallart J., Hirn A., Lépine J.-C., de Voogd B., Minshull T. A., Hello Y. and Pontoise B. (1999) Spatial distribution of hotspot material added to the lithosphere under La Réunion, from wide-angle seismic data. *J. Geophys. Res.* **104**, 2875–2893.

Clarke F. W. (1911) *The Data of Geochemistry* Bulletin 491. United States Geological Survey, Washington, p. 782.

Clocchiatti R., Havette A. and Nativel P. (1979) Relations pétrogénétiques entre les basaltes transitionnels et les océanites du Piton de la Fournaise (Ile de la Réunion, océan Indien) à partir de la composition chimique des inclusions vitreuses des olivines et des spinelles. *Bull. Minér.* **102**, 511–525.

Collins S. J., Maclennan J., Pyle D. M., Barnes S. J. and Upton B. G. J. (2012) Two phases of sulphide saturation in Réunion magma: evidence from cumulates. *Earth Planet. Sci. Lett.* **337–338**, 104–113.

Coppola D., Piscopo D., Staudacher T. and Cigolini C. (2009) Lava discharge rate and effusive pattern at Piton de la Fournaise from MODIS data. *J. Volcanol. Geotherm. Res.* **184**, 174–192.

Di Muro A., Pallister J., Villemant B., Newhall C., Semet M., Martinez M. and Mariet C. (2008) Pre-1991 sulfur transfer between mafic injections and dacite magma in the Mt. Pinatubo reservoir. *J. Volcanol. Geotherm. Res.* **175**, 517–540.

Di Muro A., Métrich N., Vergani D., Rosi M., Armienti P., Fougeroux T., Deloule E., Arienzo I. and Civetta L. (2014) The shallow plumbing system of the Piton de la Fournaise volcano (La Réunion Island, Indian Ocean) revealed by the major 2007 caldera-forming eruption. *J. Petrol.* **55**, 1287–1315.

Galer S. J. G. and Abouchami W. (1998) Practical application of lead triple spiking for correction of instrumental mass discrimination. *Mineral. Mag.* **62A**, 491–492.

Gannoun A., Vlastélic I. and Schiano P. (2015) Escape of unradiogenic osmium during sub-aerial lava degassing: evidence from fumarolic deposits, Piton de la Fournaise, Réunion island. *Geochim. Cosmochim. Acta* **166**, 312–326.

Gouhier M. and Coppola D. (2011) Satellite-based evidence for a large hydrothermal system at Piton de la Fournaise volcano (Réunion Island). *Geophys. Res. Lett.* **38**, L02302. http://dx.doi.org/10.1029/2010GL046183.

Gurioli L, Vlastélic I, Di Muro A, Boudoire G, Moune S, Bachelery P and Villeneuve N. (2015) The June 2014 eruption of Piton de la Fournaise: Insights from field, textural and geochemical data, *2015 EGU Conference,* Abstract #345

Hart S. and Gaetani G. A. (2006) Mantle Pb paradoxes: the sulfide solution. *Contrib. Mineral. Petrol.* **152**, 295–308.

Hart S. and Gaetani G. A. (2016) Experimental determination of Pb partitioning between sulfide melt and basalt melt as a function of P, T and X. *Geochim. Cosmochim. Acta* **185**, 9–20.

Harvey J., Gannoun A., Burton K., Rogers N. W., Alard O. and Parkinson I. J. (2006) Ancient melt extraction from the oceanic upper mantle revealed by Re–Os isotopes in abyssal peridotites from the Mid-Atlantic ridge. *Earth Planet. Sci. Lett.* **244**, 606–621.

Holzheid A. (2010) Separation of sulfide melt droplets in sulfur saturated silicate liquids. *Chem. Geol.* **274**, 127–135.

Jugo P. J. (2009) Sulfur content at sulfide saturation in oxidized magmas. *Geology* **37**, 415–418.

Jugo P. J., Luth R. W. and Richards J. P. (2005) An experimental study of the sulfur content in basaltic melts saturated with immiscible sulfide or sulfate liquids at 1300 °C and 1.0 GPa. *J. Petrol.* **46**, 783–798.

Larocque A. C. L., Stimac J. A. and Siebe, (1998) Metal-residence sites in lavas and tuffs from Volcan Popocatépetl, Mexico: implication for metal mobility in the environment. *Environ. Geol.* **33**, 197–208.

Larocque A. C. L., Stimac J. A., Keith J. D. and Huminicki M. A. E. (2000) Evidence for open-system behaviour in immiscible Fe–S–O liquids in silicate magmas: implication for contributions of metals and sulphur to ore-forming fluids. *Can. Mineral.* **38**, 1233–1249.

Larocque A. C. L., Stimac J. A., Siebe C., Greengrass K., Chapman R. and Mejia S. R. (2008) Deposition of a high-sulfidation Au assemblage from a magmatic volatile phase, Volcan Popocatépetl, Mexico. *J. Volcanol. Geotherm. Res.* **170**, 51–60.

Lee C.-T. A., Luffi P., Chin E. J., Bouchet R., Dasgupta R., Morton D. M., Le Roux V., Q-z Yin. and Jin D. (2012) Copper systematics in arc magmas and implications for crust-mantle differentiation. *Science* **336**, 64–68.

Lesne P., Kohn S. C., Blundy J., Witham F., Botcharnikov R. E. and Behrens H. (2011) Experimental simulation of closed-system degassing in the system basalt-H_2O–CO_2–S–Cl. *J. Petrol.* **52**, 1737–1762.

Li Y. and Audétat A. (2015) Effects of temperature, silicate melt composition, and oxygen fugacity on the partitioning of V, Mn Co, Ni, Cu, Zn, As, Mo, Ag, Sn, Sb, W, Au, Pb, and Bi between sulfide phases and silicate melt. *Geochim. Cosmochim. Acta* **162**, 25–45.

Mathez E. A. (1976) Sulfur solubility and magmatic sulfides in submarine basalt glass. *J. Geophys. Res.* **81**, 4269–4276.

Mathez E. A. (1984) Influence of degassing on oxidation states of basaltic magmas. *Nature* **310**, 371–375.

Mavrogenes J. A. and O'Neill H. S. C. (1999) The relative effects of pressure, temperature and oxygen fugacity on the solubility of sulfide in mafic magmas. *Geochim. Cosmochim. Acta* **63**, 1173–1180.

Métrich N. and Clocchiatti R. (1996) Sulfur abundance and its speciation in oxidised alkaline melts. *Geochim. Cosmochim. Acta* **60**, 4151–4160.

Moore J. G. and Calk L. (1971) Sulfide spherules in vesicles of dredged pillow basalt. *Am. Mineral.* **56**, 476–488.

Mungall J. E., Brenan J. M., Godel B., Barnes S. J. and Gaillard F. (2015) Transport of metals and sulphur in magmas by flotation of sulphide melt on vapour bubbles. *Nat. Geosci.* **8**, 216–219.

Nadeau O., Williams-Jones A. E. and Stix J. (2010) Sulphide magma as a source of metals in arc-related magmatic hydrothermal ore fluids. *Nat. Geosci.* **3**, 501–505.

Nadeau O., Stix J. and Williams-Jones A. E. (2013) The behavior of Cu, Zn and Pb during magmatic-hydrothermal activity at Merapi volcano, Indonesia. *Chem. Geol.* **342**, 167–179.

Nonell A., Toutain J.-P., Polvé M., Munoz M. and Berger G. (2005) First coupled Sr and Pb isotopic measurements in volcanic gas condensates and groundwaters of Vulcano Island (Italy). *Geochem. Geophys. Geosyst.* **6**, 11011, 10:1029/2005GC000980.

O'Neill H. S. C. and Mavrogenes J. A. (2002) The sulfide capacity and the sulfur content at sulfide saturation of silicate melts at 1400 °C and 1 bar. *J. Petrol.* **43**, 1049–1087.

Oversby V. M. (1972) Genetic relations among the volcanic rocks of Réunion: chemical and lead isotopic evidence. *Geochim. Cosmochim. Acta* **36**, 1167–1179.

Rançon J. P. (1985) Hydrothermal history of Piton des Neiges volcano (Réunion Island, Indian Ocean). *J. Volcanol. Geotherm. Res.* **26**, 297–315.

Rehkämper M., Halliday A. N., Fitton J. G., Lee D.-C., Wieneke M. and Arndt N. T. (1999) Ir, Ru, Pt, and Pd in basalts and komatiites: New constraints for the geochemical behavior of the platinum-group elements in the mantle. *Geochim. Cosmochim. Acta* **63**, 3915–3934.

Rhodes J. M. and Vollinger M. J. (2005) Ferric/ferrous ratios in 1984 Mauna Loa lavas: a contribution to understanding the oxidation state of Hawaiian magmas. *Contrib. Mineral. Petrol.* **149**, 666–674.

Sharma K., Blake S., Self S. and Krueger A. J. (2004) SO_2 emissions from basaltic eruptions, and the excess issue. *Geophys. Res. Lett.* **31**, L13612. http://dx.doi.org/10.1029/2004GL019688.

Sigmarsson O., Haddadi B., Carn S., Moune S., Gudnason J., Yang K. and Clarisse L. (2013) The sulphur budget of the 2011 Grimsvötn eruption, Iceland. *Geophys. Res. Lett.* **40**, 6095–6100. http://dx.doi.org/10.1002/2013GL057760.

Smietana M. (2011) *Pétrologie, geochronology (K–Ar) et géochimie élémentaire et isotopique (Sr, Nd, Hf, Pb) de laves anciennes de la Réunion: Implications sur la construction de l'édifice volcanique* Thèse. Université de la Réunion, France.

Stone W. E. and Fleet M. E. (1991) Nickel-copper sulfides from the 1959 eruption of Kilauea, Hawaii: contrasting compositions and phase relations in eruption pumice and Kilauea Iki lava lake. *Am. Mineral.* **76**, 1363–1372.

Strand S.R., Keith J.D., Dorais M. J., Stavast W.J.A., Aase, J., Harper M.P., Harris W.B., Syme A.K., Henderson R., Porter J. and Ashley, S.E. (2002) Mobility of copper, chlorine, and sulfur during quenching of hawaiian basaltic magmas. *2002 Denver Annual Meeting*, Abstract #36-6

Sun W., Huang R.-F., Li H., Hu Y.-B., Zhang C.-C., Sun S.-J., Zhang L.-P., Ding X., Li C.-Y., Zartman R. E. and Ling M. x. (2015) Porphyry deposits and oxidized magmas. *Ore Geol. Rev.* **65**, 97–131.

Todt W., Cliff R. A., Hanser A. and Hofmann A. W. (1996) Evaluation of a ^{202}Pb–^{205}Pb double spike for high-precision lead isotope analysis. In *Earth Processes: Reading the Isotopic Code* (eds. A. Basu and S. Hart). AGU, pp. 429–437.

Tulet P. and Villeneuve N. (2011) Large scale modeling of the transport, chemical transformation and mass budget of the sulfur emitted during the April 2007 eruption of Piton de la Fournaise. *Atmos. Chem. Phys.* **11**, 4533–4546.

Upton B. G. J., Semet M. P. and Joron J.-L. (2000) Cumulate clasts in the Bellecombe Ash Member, Piton de la Fournaise, Réunion Island, and their bearing on cumulative processes in the petrogenesis of the Réunion lavas. *J. Volcanol. Geotherm. Res.* **104**, 297–318.

Violette S., Ledoux E., Goblet P. and Carbonnel J.-P. (1997) Hydrologic and thermal modeling of an active volcano: the Piton de la Fournaise, Réunion. *J. Hydrol.* **191**, 37–63.

Vlastélic I. and Staudacher T. (2014) Iron-oxide coatings in quenched lavas from Piton de la Fournaise Volcano (Réunion Island). *2014 Goldschmidt Conference*, Abstract #1886.

Vlastélic I., Abouchami W., Galer S. J. G. and Hofmann A. W. (2001) Geographic control on Pb isotopic distribution and sources in Indian Ocean Fe–Mn deposits. *Geochim. Cosmochim. Acta* **65**, 4303–4319.

Vlastélic I., Deniel C., Bosq C., Télouk P., Boivin P., Bachèlery P., Famin V. and Staudacher T. (2009) Pb isotope geochemistry of Piton de la Fournaise historical lavas. *J. Volcanol. Geotherm. Res.* **184**, 63–78.

Vlastélic I., Staudacher T., Deniel C., Devidal J. L., Devouard B., Finizola A. and Télouk P. (2013) Lead isotopes behavior in the fumarolic environment of the Piton de la Fournaise volcano (Réunion Island). *Geochim. Cosmochim. Acta* **100**, 297–314.

Wallace P. J. and Edmonds M. (2011) The sulfur budget in magmas: evidence from melt inclusions, submarine glasses, and volcanic gas emissions. *Rev. Mineral. Geochem.* **73**, 215–246.

Warren J. M. and Shirey S. B. (2012) Lead and osmium isotopic constraints on the oceanic mantle from single abyssal peridotite sulfides. *Earth Planet. Sci. Lett.* **359–360**, 279–293.

Witt M. L. I., Mather T. A., Baker A. R., De Hoog J. C. M. and Pyle D. M. (2010) Atmospheric trace metals over the south-west Indian Ocean: total gaseous mercury, aerosol trace metal concentrations and lead isotope ratios. *Mar. Chem.* **121**, 2–16.